Received Date : 02-May-2013

Revised Date : 18-Jun-2013

Accepted Date : 26-Jun-2013

Article type : Research Article

Synthesis, Antibacterial Activities, and 3D-QSAR of Sulfone Derivatives Containing 1, 3, 4-Oxadiazole Moiety

Pei Li[1, #], Juan Yin[1, #], Weiming Xu[1], Jian Wu[1], Ming He[1], Deyu Hu[1], Song Yang[1], Baoan Song[1,*]

[1] State Key Laboratory Breeding Base of Blue Pesticide and Agricultural Bioengineering, Key Laboratory of Blue Pesticide and Agricultural Bioengineering, Ministry of Education, Research and Development Center for Fine Chemicals, Guizhou University, Huaxi District, Guiyang 550025, China

*Corresponding author: Baoan Song, E-mail:songbaoan22@yahoo.com

[#] First two authors have contributed equally to the manuscript.

This article has been accepted for publication and undergone full peer review but has not been through the copyediting, typesetting, pagination and proofreading process which may lead to differences between this version and the Version of Record. Please cite this article as an 'Accepted Article', doi: 10.1111/cbdd.12181

E-mails: pl19890627@126.com (Pei Li) yinjuan2009292018@126.com (Juan Yin) xuweiming2009@163.com (Weiming Xu) jianwu2691@yahoo.com.cn (Jian Wu) hmher@126.com (Ming He) fcc.dyhu@gzu.edu.cn (Deyu Hu) yangsdqj@126.com (Song Yang)

Abstract: A series of sulfone derivatives containing 1, 3, 4-oxadiazole moiety were prepared and evaluated for their antibacterial activities by the turbidimeter test. Most compounds inhibited growth of *Ralstonia solanacearum* (*R. solanacearum*) from tomato and tobacco bacterial wilt with high potency, among which compound **5a** and **5b** exhibited the most potent inhibition against *R. solanacearum* from tomato and tobacco bacterial wilts with EC_{50} values of 19.77 and 8.29 μg/mL, respectively. Our results also demonstrated that **5a, 5b**, and a number of other compounds were more potent than commercial bactericides Kocide 3000 and Thiodiazole Copper, which inhibited *R. solanacearum* from tomato bacterial wilt with EC_{50} values of 93.59 and 99.80 μg/mL and tobacco bacterial wilt with EC_{50} values of 45.91 and 216.70 μg/mL, respectively. The structure–activity relationship of compounds was studied using three-dimensional quantitative structure–activity relationship (3D-QSAR) models created by comparative molecular field analysis (CoMFA) and comparative molecular similarity index analysis (CoMSIA) based on compound bioactivities against tomato and tobacco bacterial wilts. The 3D-QSAR models effectively predicted the correlation between inhibitory activity and steric–electrostatic properties of compounds.

Key words: sulfone derivatives, synthesis, antibacterial activities, 3D-QSAR, CoMFA, CoMSIA

Introduction

Ralstonia solanacearum (*R. solanacearum*) is a soil-borne plant bacterial pathogen classified as one of the world's most destructive plant pathogens due to its lethality, wide host range, and broad geographic distribution. Smith proved in 1896 that bacterial wilts in many important crops such as potato, tomato, and eggplant were caused by *R. solanacearum*. *R. solanacearum* was also found to cause Granville wilt in tobacco in 1908 (1 – 2). *R. solanacearum*, a complex species belonging to the β-proteobacteria family, is currently treated by traditional bactericides such as inorganic bactericides (e.g. copper formulations). These traditional bactericides have only limited effectiveness and may induce resistance in host tobacco and tomato plants, resulting in insufficient disease control and huge economic loss. Pathogenic plant bacteria cause billions of dollars of economic loss worldwide each year and the search of more effective antibacterial agents remains a major challenge to be tackled in pesticide research (3).

Sulfone derivatives containing 1, 3, 4-oxadiazole moieties display a broad spectrum of bioactivities including antibacterial (4), antifungal (5), insecticidal (6), herbicidal (7), anticancer (8), anti-HIV-1 (9), antihepatitis (10), antitumor (11), and anti-inflammatory (12) activities. Over the past few years, the synthesis and study of bioactivity of sulfone derivatives have attracted considerable attention (4 – 12). We previously demonstrated that a

series of new 2-(methyl/ethylsulfonyl)-1, 3, 4-oxadiazole sulfone derivatives displayed potent antibacterial activities at 200 μg/mL (13). Specifically, compounds **5′c, 5′h, 5′i,** and **5′j** (**Figure 1**) showed half-maximal effective concentrations (EC_{50}) of 39.8, 60.3, 47.9, and 32.1 μg/mL in *in vitro* control of tobacco bacterial wilt caused by *R. solanacearum.* Field trials demonstrated that **5′j** achieved better control against tobacco bacterial wilt than commercial bactericide Saisentong. The structure–activity relationship (SAR) derived from antibacterial activities of compounds showed that compounds had potent antibacterial activities when the electron withdrawing group at the 3- or 4-position of phenyl was attached to the 5-position of oxadiazole (13). In our previous study, we only reported and discussed compound activities in control of *R. solanacearum* caused bacterial wilt in tobacco with very limited SAR interpretation. To continue our efforts in developing highly active and readily available bacteria inhibitors, we aimed to design and synthesize a series of methyl(ethyl) sulfone derivatives containing 1, 3, 4-oxadiazole moiety in the present study and create three-dimensional (3D) quantitative SAR (QSAR) models based on compound antibacterial activities to guide design and synthesis of more potent compounds. QSAR analysis such as comparative molecular field analysis (CoMFA) (14) has been successfully used to guide the design of new bioactive molecules (15) although it has not yet been used to design sulfone derivatives as antibacterial agents. Our bioassay results showed that some of the newly synthesized compounds demonstrated significant activities in controlling bacterial wilt in tobacco and tomato. Encouraged by these results, we performed 3D-QSAR analysis on the sulfone derivatives using CoMFA and comparative molecular similarity index analysis (CoMSIA). The effects of steric, electrostatic, hydrophobic, and hydrogen-bonding

interactions on compound activities against bacterial wilt in tobacco and tomato were determined with 3D-QSAR analysis conducted on conformationally restrained compounds including 24 newly designed and synthesized (**compounds 5a – 5x**) and 12 previously reported sulfone derivatives (**compounds 5aa – 5al**) (13, 16, 17). Predictive 3D-QSAR models for compound design and antibacterial activity forecast were also established using the SYBYL multifit molecular alignment rule. The conventional noncross-validated correlation (r^2) and cross-validated coefficients (q^2) reached 0.961 and 0.905 in CoMFA and 0.977 and 0.907 in CoMSIA for tobacco bacteria wilt control, and 0.969 and 0.961 in CoMFA and 0.971 and 0.909 in CoMSIA for tomato bacteria wilt control, respectively. The CoMFA and CoMSIA models were comparable to multifit-derived models in terms of relative descriptor field contributions and partial least-square (PLS) contour maps. It was noted that CoMSIA 3D-QSAR models, in which hydrogen-bonding interactions made large contributions to compound inhibitory activity, performed better than CoMFA models. The CoMFA and CoMSIA PLS contour maps and MOLCAD-generated active site electrostatic, lipophilic, and hydrogen-bonding potential surface maps were integrated to construct a binding mode for active site binding of sulfone inhibitors in tobacco bacterial wilt and tomato bacterial wilt. To our knowledge, the present work is the first report of sulfone compounds containing 1, 3, 4-oxadiazole moieties with potent controlling effect against tomato bacterial wilt with 3D-QSAR analysis. Further field studies on biological efficacy, crop safety, and toxicity of compounds **5a**, **5b, and 5al** as potential bactericides are in progress following regulation guidelines of pesticide registration in China.

Materials and Methods

Instruments

Melting points were determined using an XT-4 binocular microscope from Beijing Tech Instrument Co. (Beijing, China) and left uncorrected. ^{1}H and ^{13}C NMR spectra were recorded on a JEOL ECX 500 NMR spectrometer operated at room temperature and 500 MHz using $CDCl_3$ as a solvent and TMS as an internal standard. IR spectra were recorded with KBr on a Bruker VECTOR 22 spectrometer. Elemental analysis was performed on an Elemental Vario-III CHN analyzer. Reactions were monitored by thin-layer chromatography analysis on silica gel GF254. All reagents were of analytical grade or chemically pure. The physical and spectral data of compounds **5aa - 5ah** were reported in reference 13. The synthetic method and characterization data of **5ai**, **5aj,** and **5ak** were provided in reference 16 and the characterization data of **5al** were provided in reference 17.

General Synthetic Procedure

Compounds **5a to 5x** (2-(methyl/ethylsulfonyl)-5-substituted-1, 3, 4-oxadiazole) were synthesized as shown in **Scheme 1** using previously described methods (13, 16 – 18). The compounds were synthesized from substituted benzoic acid in five steps including esterification, hydrazidation, cyclization, thioetherification, and oxidation.

Preparation of 2-(Methyl/ethylsulfonyl)-5-substituted-1, 3, 4-oxadiazole (5)

2-Substituted methylthio-5-substituted-1, 3, 4-oxadiazole (0.02 mol), acetic acid (10 mL), and $KMnO_4$ (0.024 mol) were added to a 50 mL three-neck round-bottom flask equipped with a

magnetic stirrer. Reaction mixtures were stirred for 15 min at room temperature. The unreacted potassium permanganate was deoxidized by adding 10% sodium bisulfite solution in distilled water and reaction mixtures were subsequently dried under vacuum. Compounds **5a – 5x** were obtained by recrystallized from ethanol. The physical characteristics, IR, ^{1}H NMR, ^{13}C NMR, and elemental analysis data for all synthesized compounds were reported in Supporting Information. Representative data for **5a** – **5x** were shown below.

In Vitro Antibacterial Activities

Sulfone derivatives containing 1, 3, 4-oxadiazole moiety were evaluated for their antibacterial activities against tobacco bacterial wilt and tomato bacterial wilt *in vitro* by the turbidimeter test as described previously (19). In measurement of antibacterial activity in tobacco bacterial wilt, approximately 40 μL of solvent NB (1.5 g beef extract, 2.5 g peptone, 0.5 g yeast powder, 5.0 g glucose, and 500 mL distilled water; pH 7.0 – 7.2) containing tobacco bacterial wilt was added to 5 mL of solvent NB containing test compound, negative control (dimethylsulfoxide (DMSO)), or positive control (Kocide 3000 or Thiodiazole Copper). The inoculated test tubes were incubated at 30 ± 1° C with continuous shaking at 180 rpm for 24 h. The growth of bacterial culture was monitored on a spectrophotometer by measuring optical density at 600 nm (OD_{600}) and calculated by the equation: $\text{turbidity}_{\text{corrected values}} = OD_{\text{bacterial wilt}} - OD_{\text{no bacterial wilt}}$. The percent inhibition was calculated by $I\,(\%) = (C_{tur} - T_{tur})/C_{tur} \times 100$, where C_{tur} was the corrected turbidity value of bacterial culture treated with NB containing negative control (DMSO), and T_{tur} was the corrected turbidity value of bacterial culture treated with NB containing test compound or positive control. Antibacterial activity in tomato bacterial wilt was measured similarly in solvent SM (5.0 g

peptone, 2.5 g glucose, 0.5 g casein acid hydrolysate, 500 mL distilled water; pH 7.0 – 7.2) with the same negative and positive controls. EC_{50} values of compounds against tobacco bacterial wilt and tomato bacterial wilt were calculated with SPSS 17.0 software.

Datasets of QSAR

In the present work, EC_{50} values of 36 sulfone derivatives containing 1, 3, 4-oxadiazole moiety (**Scheme 1, Table 1,** and **Table 2**) against tobacco bacterial wilt and tomato bacterial wilt were determined. pEC_{50} values were calculated from EC_{50} values and presented in **Tables 1** and **2**. CoMFA and CoMSIA were performed using a training set of 26 randomly selected compounds (asterisk labeled in **Tables 3** and **4**). The 10 compounds not selected were included in the testing set.

Molecular Modeling and Alignment

Molecular modeling was performed using SYBYL 7.3 software from Tripos Inc. (St. Louis, MO, USA). All molecules were built with the SKETCH option in SYBYL under default settings. Energy minimizations were carried out using the Gasteiger–Hückel charge, Tripos force field, and Powell conjugate gradient algorithm with a convergence criterion of 0.005 kcal/mol·Å as previously described (20). pEC_{50} values of compounds were calculated as the negative logarithm of their EC_{50} values (μM) and were presented in **Tables 1** and **2**.

3D structures were aligned on common substructures and conformations of **5a** and **5b**, the most potent compound against tomato bacterial wilt and tobacco bacterial wilt, respectively. Compounds **5a** and **5b** were used as template molecules for CoMFA and CoMSIA models, respectively. The alignment results were shown in **Figure 2**.

Partial Least-Squares (PLS) Analysis

The 3D-QSAR was derived using PLS analysis in which molecules were placed in a rectangular grid and interaction energies between a probe atom and all compounds were computed at surrounding points using a volume-dependent lattice with a 2.0 Å grid spacing (default in SYBYL) to improve the signal-to-noise ratio (21). CoMFA and CoMSIA descriptors were used as independent variables and pEC_{50} values were presented as dependent variables in PLS regression analysis. 3D-QSAR was thereby carried out in two steps using the PLS technique. First, the performance of models was indicated by leave-one-out cross-validation and the optimal number of components (ONC) was determined by the highest cross-validated coefficient q^2 (20 – 27). The noncross-validated correlation coefficient r^2, standard error of estimate (SEE), and *F*-test were calculated from the second run performed without cross-validation using ONC determined in the first run (23 – 24). Contour maps of CoMFA and CoMSIA were subsequently generated with PLS coefficients as well as standard deviations of the corresponding CoMFA and CoMSIA descriptor values.

Results and Discussion

Synthesis

Compounds **5a** to **5x** were synthesized from substituted benzoic acids as depicted in **Scheme 1** in five steps including esterification, hydrazidation, cyclization, thioetherification, and oxidation. Key intermediates 2-thiol-5-substituted-1, 3, 4-oxadiazoles (**3**) were prepared by cyclization of substituted phenylhydrazide and carbon disulfide in the presence of potassium

hydroxide in ethanol under reflux conditions. The success of this reaction depended on complete removal of water after the reaction was completed because cyclization may fail in the presence of trace amounts of water. Oxadiazoles produced from cyclization reactions were subsequently converted to thioether derivatives by thioetherification. Finally, target sulfone compounds were produced by oxidation of thioethers. The physical characteristics, IR, ^{1}H NMR, ^{13}C NMR, and elemental analysis data for all synthesized compounds were reported in Supporting Information.

In Vitro Antibacterial Activities

The inhibitory effect of compounds on the growth of *R solanacearum* was studied as described in materials and methods and compound EC_{50} values for tobacco and tomato bacterial wilts were presented in **Table 1** and **2**, respectively. A significant number of compounds inhibited *R solanacearum* growth in tobacco and tomato bacterial wilts with high potency. Specifically, compounds **5a, 5b, 5g, 5q, 5ae, 5ai,** and **5al** inhibited *R solanacearum* growth in tobacco bacterial wilt *in vitro* with EC_{50} values of 21.10, 8.29, 21.02, 24.44, 18.40, 22.54, and 16.55 μg/mL, respectively. Meanwhile, compounds **5a, 5g, 5aa,** and **5ai** inhibited *R solanacearum* growth in tomato bacterial wilt with EC_{50} values of 19.77, 28.90, 31.04, and 33.74 μg/mL, respectively. Among compounds designed and synthesized in the present study, **5a** and **5b** exhibited the most potent inhibition of *R solanacearum* growth in tomato bacterial wilt and tobacco bacterial wilt with EC_{50} values of 19.77 and 8.29 μg/mL, respectively. Our results also demonstrated that **5a, 5b**, and a number of other compounds were more potent

than the commercial agent Kocide 3000 and Thiodiazole Copper, which inhibited *R solanacearum* growth in tomato bacterial wilt with EC_{50} values of 93.59 and 99.80 μg/mL and tobacco bacterial wilt with EC_{50} values of 45.91 and 216.70 μg/mL, respectively.

Performance of 3D-QSAR Models

CoMFA and CoMSIA are powerful tools used to create 3D-QSAR models based on data from known active molecules. 3D-QSAR models were created by CoMFA and CoMSIA based on experimental EC_{50} values of the 26 compounds in the training set. Predicted pEC_{50} values of compounds in both the training set and the testing set were presented together with their experimental pEC_{50} values in **Tables 3** and **4** and correlations between predicted and experimental pEC_{50} in CoMFA and CoMSIA models were presented in **Figures 3** and **4**. Overall, predicted pEC_{50} values were very close to the corresponding experimental values for compounds in both the training set and the testing set as shown in **Tables 3** and **4.** The mostly linear correlations in **Figures 3** and **4** demonstrated high predictive power of these models. Calculated statistical parameters of CoMFA and CoMSIA models were shown in **Table 5**. r^2, SEE, and F values were generated by noncross-validated PLS analyses repeated with the optimum number of components determined by cross-validated analyses. Our modeling results indicated that CoMFA and CoMSIA models built for tobacco bacterial wilt performed better than those for tomato bacterial wilt. In CoMFA and CoMSIA models for tobacco bacterial wilt, the cross-validated coefficients q^2 were 0.905 with five ONC and 0.907 with six ONC, respectively and r^2, SEE, and F values were 0.961 and 0.977, 0.109 and 0.087, and

99.808 and 132.649, respectively. The relative contributions to bioactivity from steric and electrostatic fields in the CoMFA model were 0.818 and 0.182, respectively, suggesting that bioactivity was mainly determined by steric interactions. On the other hand, the calculated contributions from steric, electrostatic, hydrophobic, H-bond donor, and H-bond acceptor fields in the CoMSIA model were 14.6%, 37.5%, 45.4%, 0%, and 2.5%, respectively, suggesting that electrostatic and hydrophobic interactions made major contributions to bioactivity.

In models built for tomato bacterial wilt, the cross-validated coefficient q^2, noncross-validated correlation coefficient r^2, SEE, and F were 0.937 with four ONC, 0.969, 0.066, and 163.664, respectively in the CoMFA model and 0.909 with six ONC, 0.971, 0.067, and 104.523, respectively in the CoMSIA model. Calculated field contributions in the same type of model were similar between tomato and tobacco bacterial wilts. In models for tomato bacterial wilt, the relative contributions from steric and electrostatic fields in the CoMFA model were 0.853 and 0.147, respectively and the relative contributions from steric, electrostatic, hydrophobic, H-bond donor, and H-bond acceptor fields in the CoMSIA model were 14.3%, 35.5%, 46.3%, 0%, and 4.0%, respectively.

Graphical Interpretation of CoMFA and CoMSIA Models

CoMFA and CoMSIA contour maps are useful tools to help interpret key structural features responsible for activity. We used contour maps to analyze how different substituents affected the inhibitory activity of sulfone derivatives.

CoMFA contour maps of the steric and electrostatic field for activities against tobacco and tomato bacterial wilts were shown in **Figure 5 and 7**, respectively. Figure **5b** was displayed with aid of visualization. Green contours in the CoMFA steric field indicated regions where bulky groups would increase activity whereas yellow contours indicated regions where bulky groups would decrease activity. Similarly, blue contours in the CoMFA electrostatic field indicated regions where electron-withdrawing groups would increase activity and red contours indicated regions where electron-donating groups would increase activity. Contour maps of the steric field in CoMFA models (**Figures 5A** and **7A**) showed several large regions of yellow contours near the 2, 3, 4-substituents of the phenyl ring and R_2 substituent group, indicating that bulky groups in these regions were disfavored. Structural features predicted in these contour maps were in alignment with experimental data showing that compound activity decreased with increase in the size of R_1 and R_2 substituent groups. Specifically, molecules with –H or –F were more potent than those with –Cl or –Br at the position of R_1 substituent group on the phenyl ring as shown in the activity order of **5b > 5c > 5e** in **Table 1** and **5ab > 5d > 5f** in **Table 2**. Similarly, replacement of methyl group with ethyl at the position of R_2 substituent group resulted in decreased activity as shown in the activity order of **5a > 5aa**, **5b > 5ab,** and **5c > 5d** in **Tables 1** and **2**. The contour map of electrostatic field in CoMFA model for tobacco bacterial wilt was illustrated in **Figure 5B** where a large region of blue contour was found near the phenyl ring, indicating that electron-withdrawing substituent groups were favored in that region. Indeed, compounds with –F at R_1 position were more potent than those with $-OCH_3$ or –H at the same position as shown in the activity order of **5b > 5o**, **5ab > 5p,** and **5b > 5a** in **Table 1**. The contour map of electrostatic field in CoMFA

model for tomato bacterial wilt was illustrated in **Figure 7B** where a large region of blue contour and two small regions of red contour were found near the 3, 4-substituents of the phenyl ring, suggesting that compounds with suitable electron-withdrawing substituent groups in these regions would likely show high antibacterial activity.

CoMSIA contour maps of steric, electrostatic, hydrophobic, and H-bond acceptor field for tobacco bacterial wilt and tomato bacterial wilt were shown in **Figure 6** and **8**, respectively, in which **6b** was also displayed with aid of visualization. The steric field map of CoMSIA showed that bulky groups in regions of green contours would increase activity whereas bulky groups in regions of yellow contours would decrease activity. Two large regions of yellow contours were found near the 4-substituent of the phenyl ring and the R_2 substituent group **in Figure 6A,** suggesting that bulky groups were disfavored in these regions. The contour maps agreed well with experimental data showing that replacement of –F with –Cl or –Br at the R_1 substituent position on the phenyl ring and replacement of methyl with ethyl at the R_2 substituent group resulted in decreased activity against tobacco bacterial wilt in the order of **5b > 5c > 5e**, **5ab > 5d > 5f**, **5a > 5aa,** and **5b > 5ab** (**Table 1**). Moreover, a large region of yellow contour was found near the 3, 4-substituents of the phenyl ring and R_2 substituent group in **Figure 8A,** suggesting that bulky groups were disfavored in that region, which was consistent with experimentally observed activity order of **5b > 5c > 5e**, **5g > 5h > 5ad,** and **5b > 5ab** (**Table 2**). Electrostatic contour maps of CoMSIA models were displayed in **Figures 6B** and **8B**, in which blue contours indicated regions where electron-withdrawing groups would increase activity and red contours indicated regions where electron-donating groups

would increase activity. A blue contour and a red contour were found in the region near the 4-substituent of the phenyl ring in **Figure 6B**, suggesting that suitable electron-withdrawing groups at the 4-substituent position of the phenyl ring would increase activity. Meanwhile, a blue contour and two red contours were found in the region near the 3, 4-substituent of the phenyl ring in **Figure 8B**, suggesting that suitable electron-withdrawing groups at the 3, 4-substituent positions of the phenyl ring would increase activity. Hydrophobic contour maps of CoMSIA models were displayed in **Figures 6C** and **8C**. Yellow and gray contours indicated regions where hydrophobic and hydrophilic groups were favored, respectively. A large region of yellow contour was found around the phenyl ring, indicating that hydrophobic groups were favored in that region, which was consistent with the prediction made from steric field maps. CoMSIA contour maps of the H-bond acceptor field were shown in **Figures 6D** and **8D** in which magenta contours near the 2-substituent position of the phenyl ring and 1, 3, 4-oxadiazole ring indicated regions where H-bond acceptor groups would increase activity.

In summary, 24 methyl(ethyl)sulfone derivatives containing 1, 3, 4-oxadiazole moiety were designed, synthesized, and evaluated for their antibacterial activities against tobacco and tomato bacterial wilts by the turbidimeter test. Our bioassay results demonstrated that a significant number of compounds exhibited excellent inhibitory effect against tobacco and tomato bacterial wilts with potencies higher than those of Kocide 3000 and Thiodiazole Copper. SAR analysis showed that compounds with small electron-withdrawing groups (e.g. –F) at the 3- and 4-position of the phenyl ring displayed high antibacterial activities against tobacco and tomato bacterial wilts. 3D-QSAR models of methyl(ethyl)sulfone derivatives

were created based on compound antibacterial activities against tobacco and tomato bacterial wilts. Predictive CoMFA and CoMSIA 3D-QSAR models for conformationally constrained methyl(ethyl)sulfone derivatives containing 1, 3, 4-oxadiazole moiety were established in which CoMSIA models performed better than CoMFA models. The 3D-QSAR models effectively predicted the correlation between antibacterial activity and steric–electrostatic properties of compounds. The present study provided further insights into the structure-based design of antibacterial compounds as potential agrochemicals.

Acknowledgment

The authors gratefully acknowledge financial support from the National Key Program for Basic Research (No.2010CB 126105) and the Key Technologies R&D Program (No. 2011BAE06 B05-6).

Abbreviations

R. solanacearum, Ralstonia solanacearum; IR, Infrared; ^{1}H NMR, ^{1}H Nuclear Magnetic Resonance; ^{13}C NMR, ^{13}C Nuclear Magnetic Resonance; EC_{50}, half-maximal effective concentration; 3D-QSAR, three-dimensional quantitative structure–activity relationship; CoMFA, comparative molecular field analysis; CoMSIA, comparative molecular similarity index analysis; NB, Nutrient Broth; SM, Semi-selective medium.

Supporting Information Description

The synthesis procedure and characterization data of compounds **5a** to **5x** were available free of charge at http://wileyonlinelibrary.com/onlineopen**.**

References

1. Salanoubat M., Genin S., Artiguenave F., Gouzy J., Mangenot S., Arlat M., Billaultk A., Brottier P., Camus J.C., Cattolico L., Chandler M., Choisne N., Claudel-Renard C., Cunnac S., Demange N., Gaspin C., Lavie M., Moisan A., Robert C., Saurin W., Schiex T., Siguier P., Thébault P., Whalen M., Wincker P., Levy M., Weissenbach J., Boucher C.A. (2002) Genome sequence of the plant pathogen *Tobacco bacterial wilt*. Nature;415:497-502.

2. Li Z.F., Wu S.L., Bai X.F., Liu Y., Lu J.F., Liu Y., Xiao B.G., Lu X.P., Fan L.J. (2011) Genome Sequence of the Tobacco Bacterial Wilt Pathogen *Tobacco bacterial wilt*. J Bacteriol;193:6088-6089.

3. Hayward A.C. (1991) Biology and epidemiology of bacterial wilt caused by *Tomato bacterial wilt*. Annu Rev Phytopathol;29:65-87.

4. Richter H.G.F., Angehrn P., Hubschwerlen C., Kania M., Page M.G.P., Specklin J.L., Winkler F.K. (1996) Design, synthesis, and evaluation of 2β-alkenyl penam sulfone acids as inhibitors of β-lactamases. J Med Chem;39:3712-3722.

5. Hiromichi I., Masakazu T., Ten U., Seiichi K. (1994) Preparation of disulfonylthiadiazoles and their use as agrochemical microbicides. JP Patent 1 994 116 252.

6. Fitzjohn S., Robinson M.P. (1994) Benzoxazole and benzothiazole derivatives. WO Patent 1 994 067 83.

7. Andrew P., Jutta E.B., Janice B., Timothy D.S. (2006) Isoxazoline derivatives and their preparation, herbicidal composition, and use as herbicides to control weeds or plant growth inhibition. WO Patent 2 006 024 820.

8. Vedula M.S., Pulipaka A.B., Venna C., Chintakunta V.K., Jinnapally S., Kattuboina V.A., Vallakati R.K., Basetti V., Akella V., Rajgopai S., Reka A.K., Teepireddy S.K., Mamnoor P.K., Rajagopalan R., Bulusu G., Khandelwal A., Upreti V.V., Mamidi S.R. (2003) New styryl sulfones as anticancer agents. Eur J Med Chem;38:811-824.

9. Silvestri R., Artico M., Regina G.L. (2004) Anti-HIV-1 activity of pyrryl aryl sulfone (PAS) derivatives: Synthesis and SAR studies of novel esters and amides at the position 2 of the pyrrole nucleus. Farmaco;59:201-210.

10. Gong P., Chai H.F., Zhao Y.F., Zhao C.S. (2006) Synthesis and in vitro anti-hepatitis B virus activities of some ethyl 5-hydroxy-1-Hindole-3-carboxylates. Bioorg Med Chem;14:2552-2558.

11. Tai X.S., Yin X.H., Tan M.Y. (2003) Crystal structure and antitumor activity of tri [2-[*N*-(4′-methyl-benzylsulfonyl) amino] ethyl]-amine. Chin J Struc Chem;22:411-414.

12. Fang S.H., Padmavathi V., Rao Y.K., Subbaiah D.R.C., Thriveni P., Geethangili M., Padaja A., Tzeng Y.M. (2006) Biological evaluation of sulfone derivatives as anti-inflammatory and tumor cells growth inhibitory agents. Int Immunopharmacol;6:1699-1705.

13. Xu W.M., Han F.F., He M., Hu D.Y., Yang S., Song B.A. (2012) Inhibition of tobacco bacterial wilt with sulfone derivatives containing 1,3,4-oxadiazole moiety. J Agri Food Chem;60:1036-1041.

14. Cramer R.D., Patterson D.E., Bunce J.D. (1988) Comparative molecular field analysis (CoMFA). 1. Effect of shape on binding of steroids to carrier proteins. J Am Chem Soc;110:5959-5967.

15. Kubinyi H. (1993) 3D QSAR in Drug Design: Theory, Methods and Applications, ed. ESCOM Science Publishers: Leiden.

16. Xu W.M., He J., He M., Han F.F., Chen X.H., Pan Z.X., Wang J., Tong M.G. (2011) Synthesis and antifungal activity of novel sulfone derivatives containing 1, 3, 4-oxadiazole moieties. Molecules;16:9129-9141.

17. Xu W.M., Yang S., Pinaki B., He J., He M., Gao L.L., Hu D.Y., Song B.A. (2011) Synthesis and bioactivity of novel sulfone derivatives containing 2, 4-dichlorophenyl substituted 1,3,4-oxadiazole/thiadiazole moiety as chitinase inhibitors. Pestic Biochem Physiol;101:6-15.

18. Chen C.J., Song B.A., Yang S., Xu G.F., Pinaki B., Jin L.H., Hu D.Y., Li Q.Z., Liu F., Xue W. (2007) Synthesis and antifungal activities of 5-(3, 4, 5-trimethoxyphenyl)-2-sulfonyl-1, 3, 4-thiadiazole and 5-(3, 4, 5-trimethoxyphenyl)-2-sulfonyl-1, 3, 4-oxadiazole derivatives. Bioorg Med Chem;15:3981-3989.

19. Paw D., Thomas R., Laura K., Karina N., Thomas A.M. (1994) Estimation of bacterial growth rates from turbidimetric and viable count data. Int J Food Microbiol;23:391-404.

20. Huang X.Y., Shan Z.J., Zhai H.L., Li L.N., Zhang X.Y. (2011) Molecular design of anticancer drug Leads based on three-dimensional quantitative structure activity relationship. J Chem Inf Mode;51:1999-2006.

21. Elizabeth A.A. and William J.W. (2006) Highly predictive CoMFA and CoMSIA models for two series of stromelysin-1 (MMP-3) inhibitors elucidate S1' and S1-S2' binding modes. J Chem Inf Model;46:1775-1783.

22. Wold S. (1978) Cross-validatory estimation of the number of components in factor and principal components models. Technometrics;20:397-405.

23. Baroni M., Clementi S., Cruciani G., Costantino G., Riganelli D., Oberrauch E. (1992) Predictive ability of regression models. Part II. Selection of the best predictive PLS model. J Chemom;6:347-356.

24. Cruciani G., Baroni M., Clementi S., Costantino G., Riganelli D., Skagerberg B. (1992) Predictive ability of regression models. Part I. Standard deviation of prediction errors (SDEP). J Chemom;6:335-346.

25. Cramer R.D., Bunce J., Patterson D., Frank I. (1988) Cross-validation, bootstrapping, and partial least squares compared with multiple regression in conventional QSAR studies. Quant Struct-Act Relat;7:18-25.

26. Jiang L.L., Tan Y., Zhu X.L., Wang Z.F., Zuo Y., Chen Q., Xi Z., Yang G.F. (2010) Design, Synthesis, and 3D-QSAR Analysis of Novel 1, 3, 4-Oxadiazol-2(3*H*)-ones as Protoporphyrinogen Oxidase Inhibitors**.** J Agri Food Chem;58:2643-2651.

27. Yang G.F. and Huang X.Q. (2006) Development of quantitative structure-activity relationships and its application in rational drug design. Curr Pharm Des;12:4601-4611.

Figure, Table, and Scheme Legends

Table 1. Inhibition effect of compounds against tobacco bacterial wilt.

Table 2. Inhibition effect of compounds against tomato bacterial wilt.

Table 3. Experimental and predicted pEC_{50} values against tobacco bacterial wilt.

Table 4. Experimental and predicted pEC_{50} values against tomato bacterial wilt.

Table 5. Statistical parameters for final CoMFA and CoMSIA models.

Figure 1. Compounds previously reported against tobacco bacterial wilt.

Figure 2. Alignment of all compounds.

Figure 3. Plots of predicted pEC_{50} versus experimental pEC_{50} against tobacco bacterial wilt. Predicted pEC_{50} values were calculated for CoMFA model (A) and CoMSIA model (B).

Figure 4. Plots of predicted pEC_{50} versus experimental pEC_{50} against tomato bacterial wilt. Predicted pEC_{50} values were calculated for CoMFA model (A) and CoMSIA model (B).

Figure 5. CoMFA contour maps of steric (A) and electrostatic (B) fields for activity against tobacco bacterial wilt.

Figure 6. CoMSIA contour maps of steric (A), electrostatic (B), hydrophobic (C), and H-bond acceptor (D) fields for activity against tobacco bacterial wilt.

Figure 7. CoMFA contour maps of steric (A) and electrostatic (B) fields for activity against tomato bacterial wilt.

Figure 8. CoMSIA contour maps of steric (A), electrostatic (B), hydrophobic (C), and H-bond acceptor (D) fields for activity against tomato bacterial wilt.

Scheme 1. General synthesis route for compounds **5a** – **5x**.

Table 1. Inhibition effect of the compounds against tobacco bacterial wilt.

No.	Compound		EC_{50}(μg/mL)	pEC_{50}(μM)	$Y = Bx + A$	R
	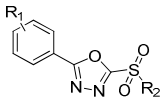					
	R_1	R_2				
5a	H	$-CH_3$	21.10 ± 0.89	4.02	$y = 1.75x + 2.68$	0.97
5b	4-F	$-CH_3$	8.29 ± 0.56	4.46	$y = 2.76x + 2.47$	0.96
5c	4-Cl	$-CH_3$	120.90 ± 2.63	3.33	$y = 1.21x + 2.47$	0.98
5d	4-Cl	$-CH_2CH_3$	471.27 ± 2.83	2.76	$y = 0.86x + 2.70$	0.99
5e	4-Br	$-CH_3$	739.62 ± 5.24	2.61	$y = 0.87x + 2.50$	0.98
5f	4-Br	$-CH_2CH_3$	1420.65 ± 7.76	2.35	$y = 1.21x + 1.18$	0.98
5g	3-F	$-CH_3$	21.02 ± 1.53	4.06	$y = 3.42x + 0.47$	0.96
5h	3-Cl	$-CH_3$	33.72 ± 1.99	3.88	$y = 2.99x + 0.43$	0.97
5i	3-Cl	$-CH_2CH_3$	147.90 ± 1.89	3.26	$y = 2.06x + 0.52$	0.99
5j	3-Br	$-CH_2CH_3$	205.39 ± 2.43	3.19	$y = 2.15x + 0.03$	0.98
5k	2-F	$-CH_2CH_3$	83.28 ± 1.82	3.49	$y = 1.54x + 2.05$	0.94
5l	2-Cl	$-CH_3$	38.98 ± 1.06	3.82	$y = 1.68x + 2.32$	0.95

5m	2-Cl	$-CH_2CH_3$	178.43 ± 0.83	3.18	$y = 1.75x + 1.05$	0.99
5n	2-Br	$-CH_2CH_3$	219.48 ± 3.26	3.16	$y = 1.99x + 0.35$	0.98
5o	4-OCH_3	$-CH_3$	74.31 ± 3.55	3.53	$y = 2.27x + 0.74$	0.95
5p	4-OCH_3	$-CH_2CH_3$	283.42 ± 3.79	2.98	$y = 1.77x + 0.66$	0.96
5q	3-OCH_3	$-CH_3$	24.44 ± 2.85	4.02	$y = 1.88x + 2.39$	0.97
5r	3-OCH_3	$-CH_2CH_3$	113.95 ± 4.21	3.37	$y = 1.74x + 1.42$	0.97
5s	2-OCH_3	$-CH_2CH_3$	134.44 ± 1.73	3.30	$y = 1.21x + 2.43$	0.99
5t	2,4-di-Cl	$-CH_2CH_3$	1448.80 ± 5.57	2.32	$y = 1.47x + 0.35$	0.95
5u	2,3-di-Cl	$-CH_3$	309.66 ± 3.55	2.97	$y = 1.66x + 0.85$	0.97
5v	2,3-di-Cl	$-CH_2CH_3$	1203.71 ± 6.75	2.41	$y = 1.66x + 0.85$	0.95
5w	3,4-di-Cl	$-CH_3$	126.00 ± 1.88	3.36	$y = 1.67x - 0.15$	0.96
5x	3,4-di-Cl	$-CH_2CH_3$	255.46 ± 2.71	2.92	$y = 1.88x + 0.48$	0.98
5aa	H	$-CH_2CH_3$	39.82 ± 4.91	3.78	$y = 3.14x - 0.02$	0.95
5ab	4-F	$-CH_2CH_3$	32.15 ± 2.34	3.90	$y = 1.81x + 2.28$	0.88
5ac	3-F	$-CH_2CH_3$	47.90 ± 3.31	3.73	$y = 3.09x - 0.30$	0.96
5ad	3-Br	$-CH_3$	52.44 ± 2.05	3.76	$y = 1.94x + 1.66$	0.98

5ae	2,4-di-F	$-CH_3$	18.40 ± 0.93	4.15	$y = 2.09x + 2.35$	0.99
5af	2,4-di-F	$-CH_2CH_3$	60.30 ± 2.82	3.66	$y = 3.81x - 1.78$	0.99
5ag	3.4-di-OCH_3	$-CH_3$	198.62 ± 2.55	3.16	$y = 1.86x + 0.73$	0.98
5ah	3.4-di-OCH_3	$-CH_2CH_3$	742.88 ± 4.21	2.60	$y = 1.27x + 1.35$	0.97
5ai	2-F	$-CH_3$	22.54 ± 1.24	4.03	$y = 1.91x + 2.42$	0.98
5aj	2-Br	$-CH_3$	75.93 ± 5.25	3.60	$y = 1.89x + 1.44$	0.96
5ak	2-OCH_3	$-CH_3$	32.40 ± 1.98	3.89	$y = 1.79x + 2.29$	0.94
5al	2,4-di-Cl	$-CH_3$	16.55 ± 1.12	4.05	$y = 3.33x + 0.25$	0.96
CK	Kocide 3000		45.91 ± 6.65	/	$y = 4.87x - 3.10$	0.98
CK	Thiodiazole Copper		216.70±5.12	/	$y = 1.03x + 2.94$	0.99

Table 2. Inhibition effect of the compounds against tomato bacterial wilt.

No.	Compound		EC_{50}(μg/mL)	pEC_{50}(μM)	$Y = Bx + A$	R
	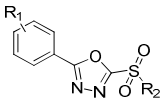					
	R_1	R_2				
5a	H	$-CH_3$	19.77 ± 0.75	4.05	$y = 2.90x + 1.24$	0.92
5b	4-F	$-CH_3$	40.13 ± 1.23	3.78	$y = 1.71x + 2.19$	0.98
5c	4-Cl	$-CH_3$	90.56 ± 2.53	3.45	$y = 1.76x + 1.55$	0.99
5d	4-Cl	$-CH_2CH_3$	139.37 ± 2.83	3.29	$y = 1.61x + 1.53$	0.99
5e	4-Br	$-CH_3$	153.53 ± 4.54	3.29	$y = 1.29x + 2.18$	0.99
5f	4-Br	$-CH_2CH_3$	228.76 ± 5.22	3.14	$y = 1.83x + 0.68$	0.99
5g	3-F	$-CH_3$	28.90 ± 1.87	3.92	$y = 1.36x + 3.01$	0.97
5h	3-Cl	$-CH_3$	56.99 ± 1.35	3.66	$y = 2.44x + 0.73$	0.99
5i	3-Cl	$-CH_2CH_3$	115.07 ± 3.11	3.37	$y = 1.46x + 1.99$	0.99
5j	3-Br	$-CH_2CH_3$	153.85 ± 4.72	3.31	$y = 1.30x + 2.15$	0.99
5k	2-F	$-CH_2CH_3$	71.09 ± 2.13	3.67	$y = 1.55x + 2.31$	0.99
5l	2-Cl	$-CH_3$	49.44 ± 1.89	3.72	$y = 2.49x + 0.78$	0.96
5m	2-Cl	$-CH_2CH_3$	118.76 ± 3.45	3.36	$y = 1.46x + 1.96$	0.99
5n	2-Br	$-CH_2CH_3$	106.71 ± 3.12	3.47	$y = 1.60x + 1.75$	0.99
5o	4-OCH_3	$-CH_3$	89.83 ± 3.57	3.35	$y = 1.82x + 1.45$	0.98
5p	4-OCH_3	$-CH_2CH_3$	159.56 ± 5.25	3.22	$y = 1.27x + 2.21$	0.98
5q	3-OCH_3	$-CH_3$	82.23 ± 2.22	3.49	$y = 1.90x + 1.35$	0.95
5r	3-OCH_3	$-CH_2CH_3$	145.83 ± 3.18	3.26	$y = 1.37x + 2.02$	0.99

5s	2-OCH_3	$–CH_2CH_3$	83.18 ± 4.75	3.51	$y = 1.80x +$	0.99
5t	2,4-di-Cl	$–CH_2CH_3$	366.88 ± 4.33	2.92	$y = 1.60x + 0.90$	0.97
5u	2,3-di-Cl	$–CH_3$	229.55 ± 3.59	3.10	$y = 1.82x + 0.70$	0.99
5v	2,3-di-Cl	$–CH_2CH_3$	505.38 ± 5.79	2.78	$y = 1.39x + 1.24$	0.95
5w	3,4-di-Cl	$–CH_3$	133.04 ± 4.70	3.32	$y = 2.91x – 1.23$	0.98
5x	3,4-di-Cl	$–CH_2CH_3$	248.04 ± 2.19	3.09	$y = 1.44x + 1.56$	0.99
5aa	H	$–CH_2CH_3$	31.04 ± 1.82	3.88	$y = 1.68x + 2.49$	0.92
5ab	4-F	$–CH_2CH_3$	43.59 ± 2.55	3.77	$y = 2.54x + 0.84$	0.97
5ac	3-F	$–CH_2CH_3$	58.80 ± 1.68	3.64	$y = 2.52x + 0.54$	0.97
5ad	3-Br	$–CH_3$	81.07 ± 2.25	3.57	$y = 1.96x + 1.26$	0.97
5ae	2,4-di-F	$–CH_3$	40.31 ± 4.16	3.81	$y = 2.03x + 1.75$	0.97
5af	2,4-di-F	$–CH_2CH_3$	90.69 ± 2.78	3.48	$y = 1.83x + 1.41$	0.98
5ag	3.4-di-OCH	$–CH_3$	253.93 ± 3.27	3.05	$y = 1.28x + 1.93$	0.99
5ah	3.4-di-OCH	$–CH_2CH_3$	527.25 ± 6.24	2.75	$y = 1.17x + 1.81$	0.99
5ai	2-F	$–CH_3$	33.74 ± 1.24	3.88	$y = 2.04x + 1.94$	0.97
5aj	2-Br	$–CH_3$	65.34 ± 2.55	3.66	$y = 2.49x + 0.48$	0.99
5ak	2-OCH_3	$–CH_3$	46.84 ± 2.87	3.73	$y = 1.85x + 1.90$	0.98
5al	2,4-di-Cl	$–CH_3$	45.47 ± 3.35	3.81	$y = 1.12x + 3.13$	0.99
CK	Kocide 3000		93.59 ± 2.17	/	$y = 1.11x + 2.80$	0.99
CK	Thiodiazole Copper		99.80 ± 4.72	/	$y = 1.03x + 2.94$	0.99

Table 3. Experimental and predicted results of pEC_{50} against tobacco bacterial wilt.

No.	Exp [a]	CoMFA		CoMSIA	
		Pred [b]	Res [c]	Pred [d]	Res
*5a	4.02	4.11	-0.09	4.15	-0.13
*5b	4.46	4.49	-0.03	4.40	0.06
*5c	3.33	3.16	0.17	3.32	0.01
*5d	2.76	2.65	0.11	2.83	-0.07
*5e	2.61	2.89	-0.28	2.74	-0.13
*5f	2.35	2.38	-0.03	2.20	0.15
*5g	4.06	4.16	-0.10	4.16	-0.10
*5h	3.88	3.87	0.01	3.85	0.03
*5i	3.26	3.36	-0.10	3.36	-0.10
*5g	3.19	3.10	0.09	3.16	0.03
*5k	3.49	3.51	-0.02	3.53	-0.04
*5l	3.82	3.67	0.15	3.74	0.08
*5m	3.18	3.19	-0.01	3.25	-0.07

***5n**	3.16	3.16	0	3.15	0.01
***5o**	3.53	3.48	0.05	3.53	0
***5p**	2.98	2.96	0.02	3.04	-0.06
***5q**	4.02	3.96	0.06	3.91	0.11
***5r**	3.37	3.44	-0.07	3.41	-0.04
***5s**	3.30	3.36	-0.06	3.37	-0.07
5t	2.32	2.25	0.07	2.42	-0.10
5u	2.97	2.93	0.04	3.02	-0.05
5v	2.41	2.43	-0.02	2.53	-0.12
5w	3.36	3.40	-0.04	3.44	-0.08
5x	2.92	2.91	0.01	2.95	-0.03
***5aa**	3.78	3.60	0.18	3.66	0.12
***5ab**	3.90	3.98	-0.08	3.91	-0.01
***5ac**	3.73	3.65	0.08	3.67	0.06
***5ad**	3.76	3.70	0.06	3.65	0.11
5ae	4.15	4.40	-0.25	4.27	-0.12

5af	3.66	3.89	-0.23	3.77	-0.11
5ag	3.16	3.04	0.12	3.48	-0.32
5ah	2.60	2.53	0.07	2.99	-0.39
***5ai**	4.03	4.02	0.01	4.02	0.01
***5aj**	3.60	3.62	-0.02	3.63	-0.03
***5ak**	3.89	3.86	0.03	3.86	0.03
5al	4.05	3.73	-0.32	3.91	0.14

[a] Experimental pEC_{50}. [b] Predicted by CoMFA. [c] Relative error of experimental predicted (*a - b/a - d*). [d] Predicted by CoMSIA. * Sample of the training set.

Table 4. Experimental and predicted results of pEC_{50} against tomato bacterial wilt.

No.	**Exp** [a]	**CoMFA**		**CoMSIA**	
		Pred [b]	**Res** [c]	**Pred** [d]	**Res**
***5a**	4.05	4.01	0.04	4.09	-0.04
***5b**	3.78	3.92	-0.14	3.87	-0.09
***5c**	3.45	3.42	0.03	3.52	-0.07

***5d**	3.29	3.19	0.10	3.29	0
***5e**	3.29	3.36	-0.07	3.27	0.02
***5f**	3.14	3.13	0.01	3.04	0.10
***5g**	3.92	3.90	0.02	3.88	0.04
***5h**	3.66	3.65	0.01	3.68	-0.02
***5i**	3.37	3.42	-0.05	3.44	-0.07
***5j**	3.31	3.33	-0.02	3.28	0.03
***5k**	3.67	3.65	0.02	3.59	0.08
***5l**	3.72	3.67	0.05	3.71	0.01
***5m**	3.36	3.44	-0.08	3.48	-0.12
***5n**	3.47	3.44	0.03	3.44	0.03
5o	3.35	3.45	-0.10	3.56	-0.21
5p	3.22	3.21	0.01	3.33	-0.11
5q	3.49	3.66	-0.17	3.49	0
5r	3.26	3.43	-0.17	3.26	0
5s	3.51	3.57	-0.06	3.52	-0.01

5t	2.92	2.86	0.06	2.91	0.01
***5u**	3.10	3.09	0.01	3.11	-0.01
***5v**	2.78	2.85	-0.07	2.88	-0.10
***5w**	3.32	3.30	0.02	3.29	0.03
***5x**	3.09	3.07	0.02	3.06	0.03
***5aa**	3.88	3.77	0.11	3.85	0.03
***5ab**	3.77	3.68	0.09	3.63	0.14
***5ac**	3.64	3.67	-0.03	3.65	-0.01
***5ad**	3.57	3.57	0	3.52	0.05
5ae	3.81	3.81	0	3.60	0.21
5af	3.48	3.56	-0.08	3.37	0.11
***5ag**	3.05	3.02	0.03	3.01	0.04
***5ah**	2.75	2.78	-0.03	2.78	-0.03
***5ai**	3.88	3.90	-0.02	3.82	0.05
***5ag**	3.66	3.69	-0.03	3.67	-0.01
5ak	3.73	3.81	-0.08	3.75	-0.02

5al	3.81	3.79	0.02	3.84	-0.03

[a] Experimental pEC_{50}. [b] Predicted by CoMFA. [c] Relative error of experimental predicted (*a* - *b/a* - *d*). [d] Predicted by CoMSIA. * Sample of the training set.

Table 5. Statistical parameters for the final CoMFA and CoMSIA models.

Statistical Parameter	**Tobacco Bacterial Wilt**		**Tomato Bacterial Wilt**	
	CoMFA	**CoMSIA**	**CoMFA**	**CoMSIA**
q^{2} [a]	0.905	0.907	0.937	0.909
ONC [b]	5	6	4	6
r^{2} [c]	0.961	0.977	0.969	0.971
SEE [d]	0.109	0.087	0.066	0.067
F_{ratio} [e]	99.808	132.649	163.664	104.523
Fraction of field contributions [f]				
Steric	0.818	0.146	0.853	0.143
Electrostatic	0.182	0.375	0.147	0.355
Hydrophobic		0.454		0.463

Donor	0	0
Acceptor	0.025	0.040

[a] Cross-validated correlation. [b] Optimum number of components. [c] Noncross-validated correlation. [d] Standard error of estimate. [e] *F*-test value. [f] Field contributions: steric, electrostatic, hydrophobic, H-bond donor, and H-bond acceptor.

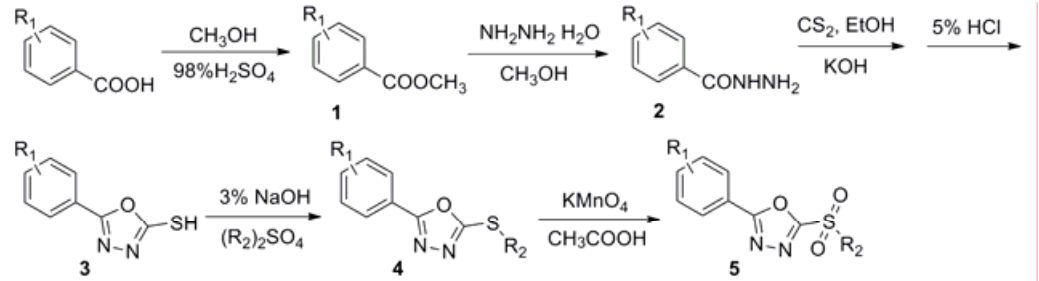

5a. R_1 = H, R_2 = $-CH_3$; 5b. R_1 = 4-F, R_2 = $-CH_3$; 5c. R_1 = 4-Cl, R_2 = $-CH_3$;

5d. R_1 = 4-Cl, R_2 = $-CH_2CH_3$; 5e. R_1 = 4-Br, R_2 = $-CH_3$; 5f. R_1 = 4-Br, R_2 = $-CH_2CH_3$;

5g. R_1 = 3-F, R_2 = $-CH_3$; 5h. R_1 = 3-Cl, R_2 = $-CH_3$; 5i. R_1 = 3-Cl, R_2 = $-CH_2CH_3$;

5j. R_1 = 3-Br, R_2 = $-CH_2CH_3$; 5k. R_1 = 2-F, R_2 = $-CH_2CH_3$; 5l. R_1 = 2-Cl, R_2 = $-CH_3$;

5m. R_1 = 2-Cl, R_2 = $-CH_2CH_3$; 5n. R_1 = 2-Br, R_2 = $-CH_2CH_3$; 5o. R_1 = 4-OCH_3, R_2 = $-CH_3$;

5p. R_1 = 4-OCH_3, R_2 = $-CH_2CH_3$; 5q. R_1 = 3-OCH_3, R_2 = $-CH_3$; 5r. R_1 = 3-OCH_3, R_2 = $-CH_2CH_3$;

5s. R_1 = 2-OCH_3, R_2 = $-CH_2CH_3$; 5t. R_1 = 2,4-di-Cl, R_2 = $-CH_2CH_3$; 5u. R_1 =2,3-di-Cl, R_2 = $-CH_3$;

5v. R_1 = 2,3-di-Cl, R_2 = $-CH_2CH_3$; 5w. R_1 = 3,4-di-Cl, R_2 = $-CH_3$; 5x. R_1 = 3,4-di-Cl, R_2 = $-CH_2CH_3$.

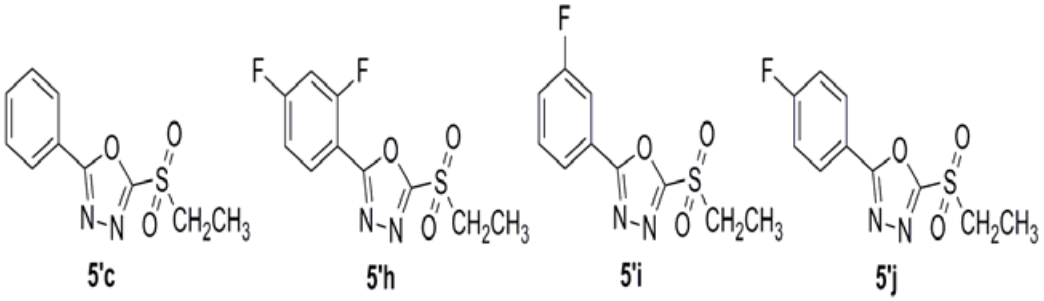

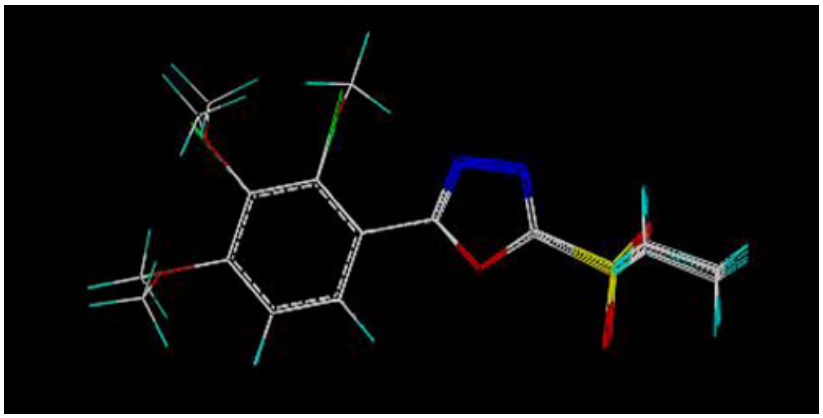

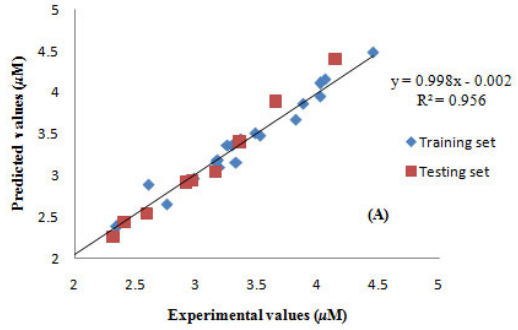

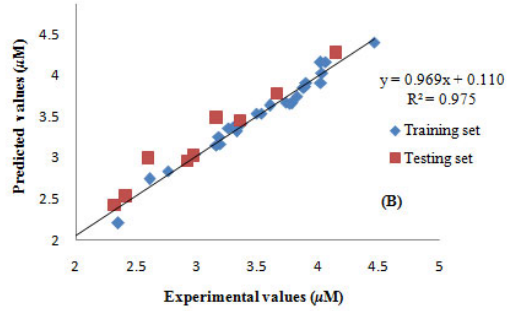

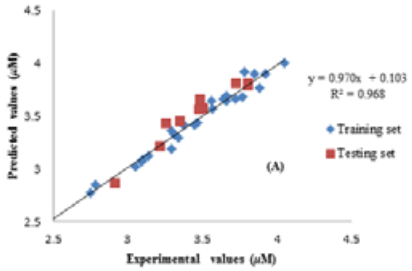

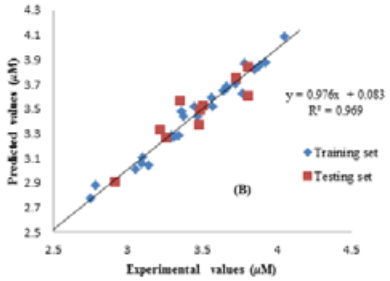

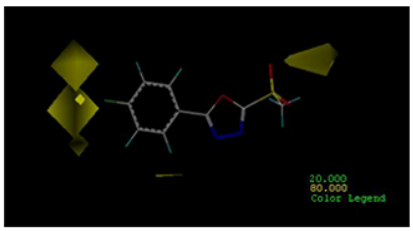

A

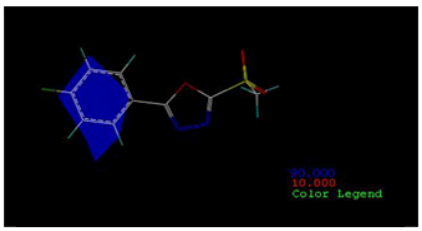

B

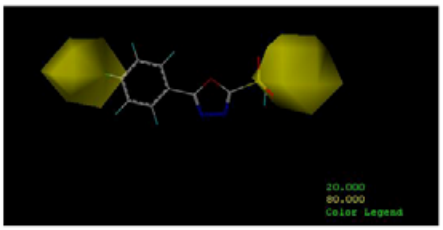

A

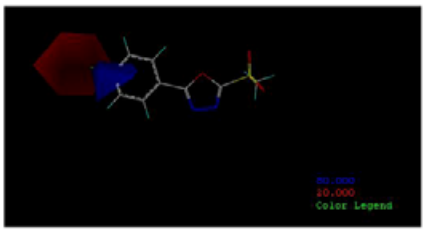

B

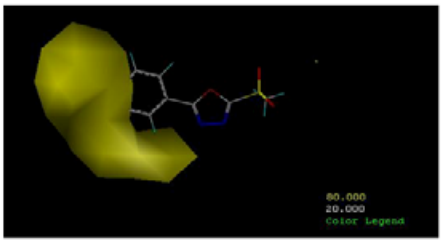

C

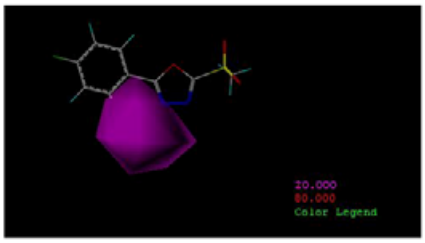

D

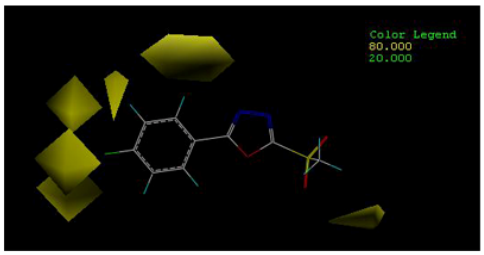

A

B